Version of Record: https://www.sciencedirect.com/science/article/pii/S0377042721006324
Manuscript_d83ad3cb0e8208a1a86ce2a1f79fce07

Schemes for cubature over the unit disk found via numerical optimization

Nick Takaki[1,2,*], G. W. Forbes[3,**], and Jannick P. Rolland[1,***]

[1]*University of Rochester, The Institute of Optics, 480 Intercampus Drive, Rochester, NY, 14627, USA*
[2]*Synopsys, Inc., 11 Apex Drive, Marlborough, MA, USA 01752*
[3]*Macquarie University, Department of Physics and Astronomy, North Ryde 2109, Sydney, New South Wales, Australia*
**nicktakaki@gmail.com, Corresponding Author*
***forbes@bigpond.net.au*
****rolland@optics.rochester.edu*

Abstract

Cubature schemes, in this case for uniformly weighted integration over the unit disk, enable exact evaluation of numerical integrals of polynomials but have been explicitly constructed for only low or moderate degrees. In this paper, cubature formulae are discovered for a wider range of degrees by leveraging numerical optimization. These results include a degree-17 cubature scheme with fewer points than existing solutions and up to a degree-77 solution with 1021 cubature points. Optimization heuristics and patterns in the distributions of cubature points are discussed, which serve as vital guides in this work. For example, these heuristics leverage a connection to circle-packing configurations to facilitate the discovery of fully symmetric cubature schemes.

Keywords: Cubature Formulas; Numerical Integration; Unit Disk; Least-Squares Optimization

1 Introduction

A standard approach for numerically approximating integrals is to develop schemes that are exact for polynomials up to degree T with a modest number of sample points. To integrate a polynomial f on a domain Ω with an integration weight function w, the goal is then to make a careful selection of the sample points $u_j \in \Omega$ and sample weights $W_j > 0$ such that

$$\sum_j W_j f(u_j) - \int_{u\in\Omega} f(u)w(u)du = 0 \quad \forall f \in \mathcal{P}_T, \tag{1}$$

where $\mathcal{P}_T$ is the space of polynomials of degree at most T and w is strictly positive. The sum is then used to estimate the integral more generally. For efficiency, it is preferable to use as few points as possible to achieve exact integration up to degree T.

When Ω is a one-dimensional interval (WLOG, say [-1,1]), Gaussian quadrature rules solve the $2n$ equations corresponding to Eq. (1) for all polynomials of degree at most $2n-1$ with exactly the $2n$ unknowns corresponding to the locations and weights of n quadrature points. It turns out that the locations lie within the interval Ω and the weights are all positive. The quadrature schemes corresponding to $w(u) = 1$ and $w(u) = \frac{1}{\sqrt{1-u^2}}$, known as Legendre-Gauss and Chebyshev-Gauss quadrature, respectively, serve as motivation for the optimization heuristics discussed in Section 2.2.2 of this paper.

If Ω is increased in dimension – in this paper, to the unit disk – the task of quadrature becomes the task of cubature. For more general domains and weights, it has been shown that the number of points needed for cubature can be bounded below based on the degree of the polynomials to be integrated and the dimension of Ω ([1, 2]). Cubature schemes attaining these bounds are sometimes referred to as "Gaussian" (see, e.g., [3-5]). However, rules that achieve these lower bounds are rare and often specific to the domain and weight of integration [4, 6-12].

We choose to focus specifically on cubature over the unit disk with uniform integration weight, for which the bounds on the number of necessary cubature points can be tightened [2]. While symbolic methods exist for generating cubature

formulae on the disk (see, e.g., [5, 13]), only low- or moderate-degree cubature schemes that achieve or nearly achieve this lower bound are constructed with explicit numerical representations. For example, in the review of near-minimal cubature formulae in [5], the highest-degree cubature rules are the degree-17 scheme with 57 cubature points by Cools and Kim [14] and the degree-19 rule with 72 points of Kim and Song [15]. Similarly, in Cools' review of existing cubature formulas, which is not limited to cubature schemes for uniform integration weight, the highest-degree rule for integration over the unit disk is of degree 31 [16]. More recently, Forbes et al. show solutions up to a degree-25 solution with 117 cubature points [17], while Forbes and Ruoff include solutions up to degree 39 with as few as 275 cubature points [18].

In this paper, we construct cubature schemes of moderate and high degree over the domain of the unit disk with a uniform weight function. Rather than attempting to be near minimal in the sense of [2], we instead take inspiration from Gaussian quadrature for which the number of unknowns is equal to the number of polynomials to be integrated. In particular, given that there are $\binom{T+2}{2}$ monomials $x^j y^k$ with $j + k \leq T$, we adopt an *efficiency criterion* (EC) that the number of sample points J in a cubature scheme of degree T should satisfy

$$J \leq \chi(T) \coloneqq \left\lceil \binom{T+2}{2} / 3 \right\rceil. \tag{2}$$

The division by three reflects the fact that each sample point can introduce three cubature parameters (namely two for location and one for weight), and a "round up" operation is permitted in Eq.(2) to ensure an integer as the resulting upper bound on J. Note incidentally that $\chi(17) = 57$, which is precisely the number of points in the near-minimal cubature solution of Cools and Kim [14]. We show in Section 3, however, that it is possible to do even better than what is required by this EC. For the purpose of context setting, it is also noteworthy that some of the schemes mentioned in the previous paragraph fail to meet the EC.

To find these cubature schemes, we leverage least-squares optimization methods to solve Eq. (1) by constructing a residual whose elements are the difference between the exact and numerically estimated integral of each polynomial. In this way, the task of finding cubature schemes is reduced to root finding. Numerical approaches like least-squares optimization have been used to seek cubature schemes over other domains, such as triangular domains by Taylor et al. [19] and by Papanicolopulos [20], triangular and tetrahedral domains by Zhang et al. [21], and over a variety of polygonal and polyhedral domains by Witherden and Vincent [22]. With this approach, we find cubature schemes over the unit disk that meet or improve upon the EC of Eq. (2), ranging from a degree-17 cubature scheme with only 55 cubature points (two fewer than the 57-point rule of [14]) to a degree-77 cubature scheme that integrates 3081 monomials with $J = 1021$ —six fewer than $\chi(77)$. The schemes reported below all meet the EC and either use fewer cubature points or integrate polynomials up to a higher degree than existing published results. The coordinates and weights of these cubature points are provided as an online supplement to this paper, and fascinating patterns in the solutions are discussed.

2 Cubature as zero-error least-squares solutions

2.1 Error and point count requirements for cubature schemes

We seek positive-weight cubature schemes whose samples lie within the domain of integration that exactly integrate all polynomials of degree up to T over the unit disk with uniform integration weight using at most $\chi(T)$ samples. This search is reduced to a least-squares optimization problem whose optimization variables are the locations and weights of the cubature points and whose residual is comprised of the differences between the estimated and analytic integrals of each polynomial of degree up to T. That is, for a polynomial $f \in \mathcal{P}_T$, the contribution R_f to the residual $\boldsymbol{R}$ is

$$R_f = \sum_j W_j f(u_j, \theta_j) - \iint_{(u,\theta)\in\Omega} f(u,\theta)\ u\ dud\theta, \tag{3}$$

and a cubature scheme of degree T makes the following vanish

$$E^2 = \boldsymbol{R}^T \boldsymbol{R} = \sum_{f\in\mathcal{P}_T} \left[\sum_j W_j f(u_j, \theta_j) - \iint_{(u,\theta)\in\Omega} f(u,\theta)\ u\ dud\theta \right]^2. \tag{4}$$

In this way, cubature schemes can be sought by leveraging numerical optimization techniques initialized with non-exact configurations.

Since some applications seek to integrate functions with singularities on the boundary, schemes whose points do not lie on the boundary are preferred in this paper. Accordingly, we have endeavored to maximize the distance of sample points from the boundary.

In practice, while initializations with $\chi(T)$ points can sometimes be optimized to find cubature schemes that meet our EC, we often had greater success by starting with more points, optimizing to find an exact solution, and then iteratively removing points and re-optimizing until a scheme with at most $\chi(T)$ points was found. While the determination of when to remove points and which points to remove was ultimately based on author discretion, the heuristics discussed in Section 2.2.2 and the exploration of continuums of solutions discussed in Section 2.2.3 proved useful when seeking high-degree cubature schemes (although there is admittedly a chance that they create a self-fulfilling prophecy).

As a final observation, note that the cubature weights enter linearly into the residuals and, consequently, their values can be determined by using standard linear least-squares techniques that minimize the root-sum-square error. Specifically, if $\boldsymbol{Z}$ is the matrix of evaluations of the polynomials $f \in \mathcal{P}_T$ at the points (u_j, θ_j), so that each row is $\{f(u_j, \theta_j)\}$ for a given f, $\boldsymbol{\epsilon} = \left\{\iint_{(u,\theta)\in\Omega} f(u,\theta)\ u\ dud\theta\right\}$ is a vector containing the exact integrals of each polynomial and $\boldsymbol{w} = \{w_j\}$ is a vector of the weights, then the vector of residuals $\boldsymbol{R}$ can be written as

$$\boldsymbol{R} = \boldsymbol{Z}\boldsymbol{w} - \boldsymbol{\epsilon} \tag{5}$$

and the weights are calculated as

$$\boldsymbol{w} = \boldsymbol{Z}^{+}\boldsymbol{\epsilon}, \tag{6}$$

where $\boldsymbol{Z}^{+}$is the Moore-Penrose pseudo-inverse of $\boldsymbol{Z}$ (see, for example, [23, 24]). This helpfully reduces the dimensionality of the remaining optimization task.

For deriving the results in this paper, one of the authors used Mathematica while another author used MATLAB in much the same way. In MATLAB, for example, the LSQNONLIN function (configured to use the Levenberg-Marquardt algorithm) was used for optimization while the weight evaluation employed the PINV function (which evaluates a pseudo-inverse) [25, 26]. Both software packages were successful at achieving the results in this paper.

2.2 Optimization guidelines and rules of thumb

2.2.1 Orthogonal basis for $\mathcal{P}_T$ and symmetry

While, in principle, any basis set can be used for $\mathcal{P}_T$ in Eq. (1), it is numerically advantageous to adopt an orthogonal basis because the associated recurrence relations allow the computations to be less impacted by round-off. It is also convenient that the integral of every polynomial beyond the degree-zero constant is then exactly zero. Accordingly, we have followed upon [17, 18] and chosen to use Zernike polynomials [27-29] as a basis set for $\mathcal{P}_T$. The requirement for cubature is thus

$$\begin{gathered}
\sum_{j=1}^{J} W_j P_n^{(0,m)}\left(2u_j^2 - 1\right) {u_j}^m \cos\left(m\theta_j\right) = \iint_{(u,\theta)\in\Omega} P_n^{(0,m)}(2u^2 - 1)u^m \cos(m\theta)\, udud\theta = 0, \\
\sum_{j=1}^{J} W_j P_n^{(0,m)}\left(2u_j^2 - 1\right) {u_j}^m \sin\left(m\theta_j\right) = \iint_{(u,\theta)\in\Omega} P_n^{(0,m)}(2u^2 - 1)u^m \sin(m\theta)\, udud\theta = 0, \\
\text{for } 1 \le m + 2n \le T, \\
\sum_{j=1}^{J} W_j P_n^{(0,m)}\left(2u_j^2 - 1\right) = \iint_{(u,\theta)\in\Omega} P_n^{(0,m)}(2u^2 - 1)\ u\ du\ d\theta = \pi, \\
\text{for } m = n = 0,
\end{gathered} \tag{7}$$

where $P_n^{(0,m)}$ is a Jacobi polynomial [30]. Note that $P_n^{(0,m)}(2u^2-1)u^m\cos(m\theta)$ and $P_n^{(0,m)}(2u^2-1)u^m\sin(m\theta)$ are both of degree $m+2n$. For the last line in Eq. (7), note that $P_0^{(0,0)}(x)\equiv 1$.

It follows from the trigonometric contributions in Eq. (7) that cubature schemes possessing symmetry with respect to rotational segments or a plane of reflection always approximate the integral of many Zernike polynomials to the correct value of zero. For example, a cubature scheme possessing six-fold rotational segmentation evaluates the numerical integral of all Zernike polynomials to zero automatically, except those whose azimuthal dependence involves an integer multiple of six. Similarly, if a cubature scheme is reflection symmetric (WLOG, about $\theta=0$), then the integrals of all Zernike polynomials with sinusoidal trigonometric dependence also automatically evaluate to zero.

Rotational segmentation and reflection symmetry therefore not only reduce the number of sample points but also the number of polynomials that need to be handled. This reduction becomes increasingly advantageous when seeking higher-degree cubature schemes. For a scheme with *k*-fold rotational segmentation and for which $\sigma_{\text{Refl}}=1$ when the scheme has a plane of reflection symmetry and is zero otherwise, the symmetry-reduced least-squares error function becomes:

$$E_{\text{Sym}}^2 = R_{\text{Sym}}^T R_{\text{Sym}} = \left[\sum_j W_j - \frac{\pi}{k}\right]^2 + \sum_{1\le km+2n\le T}\left[\sum_j W_j P_n^{(0,km)}(2u_j^2-1){u_j}^{km}\cos\left(km\theta_j\right)\right]^2 + (1-\sigma_{\text{Refl}})\sum_{1\le km+2n\le T}\left[\sum_j W_j P_n^{(0,km)}(2u_j^2-1){u_j}^{km}\sin\left(km\theta_j\right)\right]^2. \quad (8)$$

Note that while the sum over j in Eq. (8) ranges over the reduced subset of points in a single segment, we require cubature schemes to use at most $\chi(T)$ cubature points over the whole disk, regardless of whether they possess rotational segmentation or reflection symmetry. The number of optimization variables and the number of polynomials that contribute to the residual are counted with reference to Eq. (8), whereas the number of cubature points and the number of monomials of degree T are counted over the full disk.

2.2.2 Warped coordinates and weight estimates for quadrature & cubature

Because the optimization problem in hundreds of dimensions for finding efficient, high-degree cubature schemes is so challenging, we begin by noticing patterns in the known solutions for Chebyshev-Gauss and Legendre-Gauss quadrature. When evaluating 1D integrals with an integration weight of $w(u)=\frac{1}{\sqrt{1-u^2}}$, the Chebyshev-Gauss quadrature solution with J points has an elegant closed form (see, e.g., [31]):

$$u_j = \cos\left(\tfrac{(2j-1)\pi}{2J}\right); \qquad W_j = \frac{\pi}{J} \quad (9)$$

for $j=1,\ldots,J$. Figure 1(a) graphically represents the Chebyshev-Gauss quadrature scheme for $J=19$, with the area of each point scaled to be proportional to the cubature weight; hence, they are all uniformly sized. By transforming the locations of the points via $\omega:=\frac{2}{\pi}\arcsin(u)$, Chebyshev-Gauss quadrature schemes can be seen to sample the warped space uniformly; see, for example, Figure 1b.

Figure 1. For J=19, locations of the Chebyshev-Gauss quadrature points are shown in (a), while in (b) the locations use a warped coordinate.

More strikingly, Legendre-Gauss quadrature schemes, which evaluate 1D integrals with an integration weight of $w(u)=1$, are also approximately uniformly distributed when viewed with the same transformation $\omega=\frac{2}{\pi}\arcsin(u)$. Further, scaling the Legendre-Gauss quadrature weights by dividing them by $\frac{\pi}{J}\sqrt{1-u^2}$ leads to a representation in

which the scaled weights are also approximately uniform. Figure 2 shows the Legendre-Gauss cubature points (a) in standard and (b) transformed coordinates. In Figure 2a, the areas of the points are proportional to the cubature weights, while in Figure 2b these weights are normalized by $\frac{\pi}{J}\sqrt{1-u^2}$ and can be seen to be approximately uniform in size.

Figure 2. For J=19, locations of the Legendre-Gauss quadrature points are shown in (a), while in (b) the locations use a warped coordinate. In (a), the area of each point is proportional to the Legendre-Gauss quadrature weight, while in (b) the weights are normalized by $\frac{\pi}{J}\sqrt{1-u^2}$.

Inspired by this observation, we looked for a similar coordinate transformation and weight estimate for cubature schemes for the disk. Following upon [17, 18], we observed that the cubature points are roughly uniformly distributed on a warped unit disk where the azimuthal angle is preserved but with a new radial coordinate defined by

$$\omega := \frac{2}{\pi}\arcsin(u). \tag{10}$$

Similarly, we have seen that the weight as a function of the (unwarped) radial coordinate, u, can typically be fitted well by appropriately choosing values for a and b in an expression of the form

$$\frac{a}{J}(1-u^2)^b, \tag{11}$$

where, recall, J is the number of sample points employed by the cubature scheme.

Especially for any cubature scheme that has all points within the disk (i.e., none on the rim), it can be informative to represent the scheme graphically by using the warped radial coordinate to determine the cubature points' locations, say (ω_j, θ_j), and choosing the area of each point to be proportional to its weight value, say W_j, divided by the approximation given by the fitted form of Eq. (11). This representation enables a visual inspection to assess the overall scheme: regions where the points are less uniformly distributed or have more significant variations in size often highlight locations where possible improvements may be made or where cubature points can be removed. Such pointers have proven useful when seeking high-degree cubature schemes.

2.2.3 Families of solutions

It turns out that many of the cubature schemes presented in this paper are not isolated solutions but instead belong to continuous families of similar schemes. In particular, given a zero-error solution for which the number of optimization variables exceeds the number of polynomials contributing to the residual, there is generally a set of differential displacements that, to second order, preserves the error value of zero (see Appendix C for calculation of these differential displacements). In such cases, adjusting the original solution by these differential displacements creates a new non-exact configuration that, when reoptimized, often leads to new schemes that differ from the original by approximately the differential displacement.

Where possible, we explored such continuums of solutions with the goal of reducing the overall number of cubature points, such as by applying displacements that facilitate the combination of two cubature points or that remove a point by reducing its weight to zero. If we could not reduce the number of points, we endeavored to maximize the distance of cubature points to the boundary. For all solutions, δ reports the dimensionality of the family. Further, when presenting results in Section 3, if a cubature scheme is a member of a continuum of solutions, we also show δ sets of differential displacements that serve as a basis for locally generating the associated δ-dimensional family. Graphical representations of these displacements are presented using the warped radial coordinate of Eq. (10).

3 Specific solutions

3.1 Spiraled solutions

In this section, cubature schemes with spiraled distributions with six-fold rotational symmetry are constructed, first for moderate degrees and then for high degrees. Additional solutions are relegated to Appendix A.

3.1.1 T=17 solution

For $T = 17$, there are $\binom{17+2}{2} = 171$ monomials to integrate and our EC is that $J \leq \chi(17) = 57$. As noted in Section 2.2.1, if we seek a cubature scheme with six-fold rotational segmentation and we represent these monomials in terms of Zernike polynomials, then only those Zernike polynomials whose azimuthal orders are multiples of six need to be considered. In particular, there are nine rotationally symmetric polynomials that must be considered, $2 \times 6 = 12$ of azimuthal order six, and $2 \times 3 = 6$ of azimuthal order twelve, which make for a total of 27 conditions that must be met; rotational segmentation ensures that the estimated integrals of all other (non-constant) Zernike polynomials of degree up to 17 evaluate exactly to the desired value of zero. If an irrelevant global rotation is used to arbitrarily fix the azimuthal angle for one of the off-center samples, there are 27 optimization variables in a scheme that includes a sample at the origin and nine off-center samples (eight of which have three degrees of freedom each, one with two, and the only freedom for the central point is its weight). It turns out that this set of 27 highly non-linear equations in 27 unknowns possesses at least one isolated solution (i.e., $\delta = 0$), see Figure 3. The six-fold rotational segmentation permits a configuration that transitions from a pattern of nearly isometric triangles near the center to a pattern of approximately evenly spaced rings nearer to the perimeter. Impressively, this solution involves only $6 \times 9 + 1 = 55$ points; that is, two fewer than the upper bound set by our EC. To allow comparison of efficiency across schemes with different degrees, this improvement over our EC is expressed in percent via $\beta = \frac{\chi(T)-J}{\chi(T)}$, and in this case is $\beta = \frac{2}{57} = 3.5\%$. Importantly, diagrams like that of Figure 3 allow all 27 degrees of freedom to be assessed at a glance. Figure 3(b) shows the normalized view of these schemes discussed in Section 2.2.2; we have come to expect the points to be roughly uniformly distributed and sized in this normalized view.

Table 1 reports the coordinates and weights of the sample points in the marked segment of the cubature scheme reported in Figure 3. Replication generates the entire scheme. For all cubature schemes in this paper, numerical values for the coordinates and weights are reported in an online supplement to this paper in a similar fashion to that in Table 1. A numerical test of the exactness of this cubature scheme is presented in Appendix D.

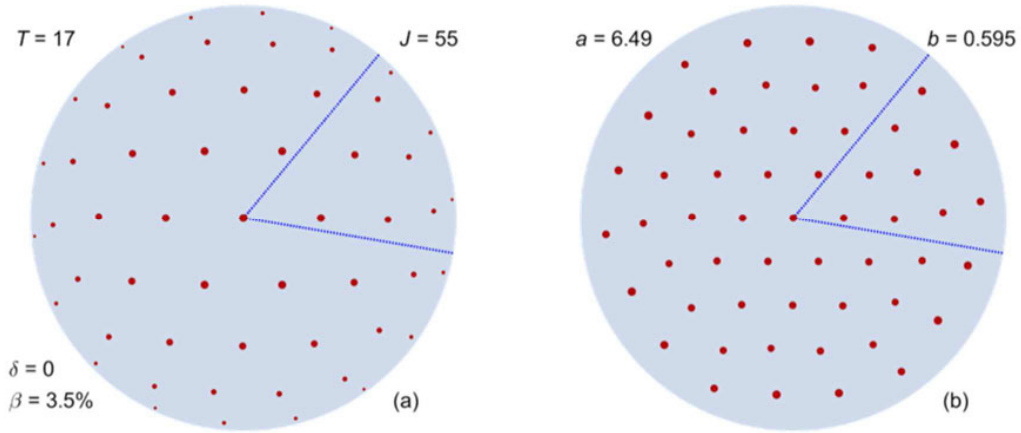

Figure 3. A cubature scheme for degree 17 with 55 sample points is shown in (a), where the area of each point is proportional to its associated weight. This solution is isolated (hence $\delta = 0$) and beats the EC by $\beta = 3.5\%$. The warped radial coordinate is used in (b), where the weights are normalized by the expression $\frac{a}{J}(1-u^2)^b$ with $a = 6.49$ and $b = 0.595$. The dotted lines in this six-fold symmetric pattern mark out the arbitrarily oriented segment corresponding to the sample points in Table 1. Note that mirror imaging trivially generates a counter-rotating solution for any spiraled scheme.

Table 1. One segment of a six-fold symmetric cubature scheme for degree 17, corresponding to those points in the marked region of Figure 3. These tabulated weights sum to $\pi/6$ and the weight of the central point is effectively multiplied by six under replication to generate the entire scheme. The locations and weights were calculated with double-precision, so the very last of the fifteen digits is included for completeness but may not necessarily be correct.

j	u_j	θ_j	W_j
0	0	0	0.019985648352286
1	0.363775420550028	0	0.109390374900056
2	0.601744604816974	0.518032211681943	0.089605867922125
3	0.678087439319387	−0.010917514653234	0.080901543010582
4	0.827920982305579	0.355384455969964	0.054662924040364
5	0.842372199542979	0.724984830394064	0.056341227935879
6	0.893306018833271	0.038507776114625	0.042520120571368
7	0.965628629843171	0.429897101117210	0.029311953277726
8	0.972104010066202	0.778946956506373	0.024671001837889
9	0.982771494440792	0.089653787780584	0.016208113750023

3.1.2 T=21 solution

A second moderate-degree scheme of this type offers some further helpful observations. In the case of degree 21, there are $\binom{21+2}{2} = 253$ monomials, and we seek a cubature scheme with $J \leq \chi(21) = 85$. Much as described for the case of $T = 17$ above, when Zernike polynomials are used together with six-fold rotational segmentation, there are now $11 + 2 \times (8 + 5 + 2) = 41$ conditions that must be met. After removing an irrelevant global rotation, there are 42 optimization variables in a scheme that includes a sample at the origin and fourteen off-center samples. Such a configuration would just meet the requirement of no more than 85 cubature points in the disk. Although no solution is guaranteed, it was found that this set of 41 equations in 42 unknowns possesses a one-parameter family of solutions (i.e., $\delta = 1$). A representative member is shown in Figure 4, and another striking member is depicted in Figure 5. The differential displacements, discussed in Section 2.2.2, for each of these solutions are shown in Figure 6. By applying these differential displacements and reoptimizing, a continuum of solutions can be found that connects the solution of Figure 4 to the solution of Figure 5. That is, it is possible to find a solution with a plane of reflection symmetry, and then also find solutions that continuously connect configurations with counterclockwise spirals to those with clockwise spirals (compare the sense of the spirals in Figure 3 and Figure 4). Notice that the specific family member is identified by the choice of $\theta_{14} = -0.15$ (and this becomes either $\theta_{11} = 0$ or, equivalently $\pi/3$, for the spiral-free case in Figure 5).

Unlike the isolated cubature scheme of degree 17 discussed earlier, this family of cubature schemes of degree 21 simply meets but does not beat our EC. While redundant optimization variables are ideally exploited to eliminate sample points, we were not always able to do so in practice. Interestingly, if reflection symmetry is analogously forced upon a segment of the solution for degree 17, there are 18 conditions to meet with only 17 remaining degrees of freedom, and there appears to be no solution.

Note finally that, like the $T = 17$ solution, both solutions adopt configurations that transition from a pattern of nearly isometric triangles near the center to a pattern of approximately evenly-sampled rings nearer the perimeter.

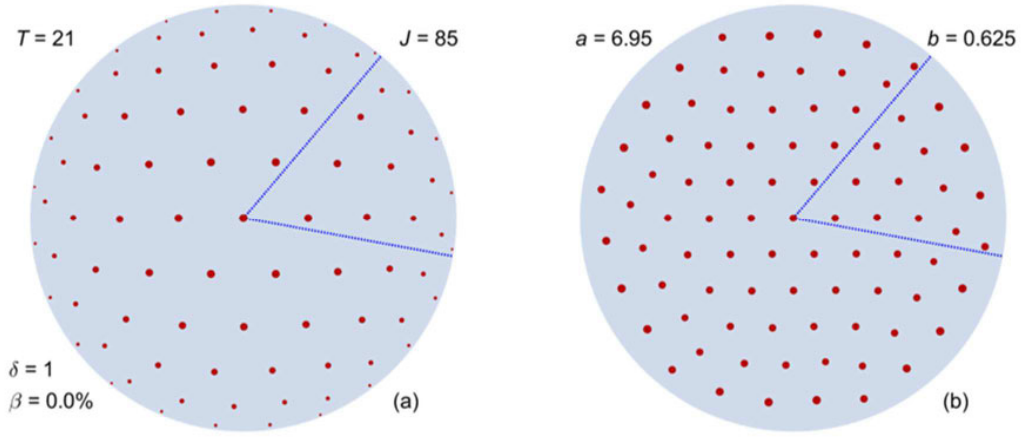

Figure 4. In the representation introduced in Figure 3, a cubature scheme for degree 21 with 85 sample points is shown in (a), which is a member of a one-dimensional family of solutions (i.e., $\delta = 1$) that exactly meets the efficiency criterion (i.e., $\beta = 0.0\%$). The normalized depiction is in (b) with $a = 6.95$ and $b = 0.625$.

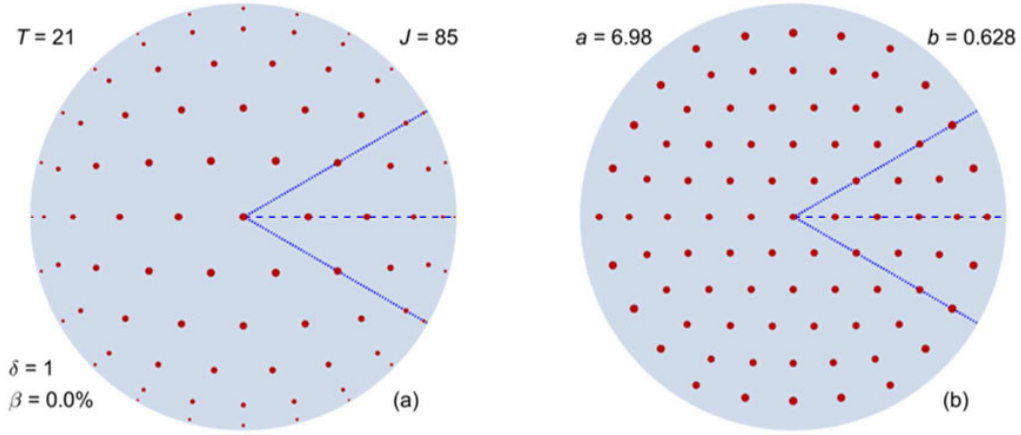

Figure 5. A reflection-symmetric configuration for degree 21 using 85 sample points with $\delta = 1$ and $\beta = 0\%$ is shown in (a), and the normalized depiction is in (b) with $a = 6.97$ and $b = 0.625$. The dotted lines highlight a segment with internal symmetry. If this symmetry is explicitly enforced, there are then only $11 + 8 + 5 + 2 = 26$ conditions to be met and precisely 26 degrees of freedom available (14 position coordinates and 12 weights).

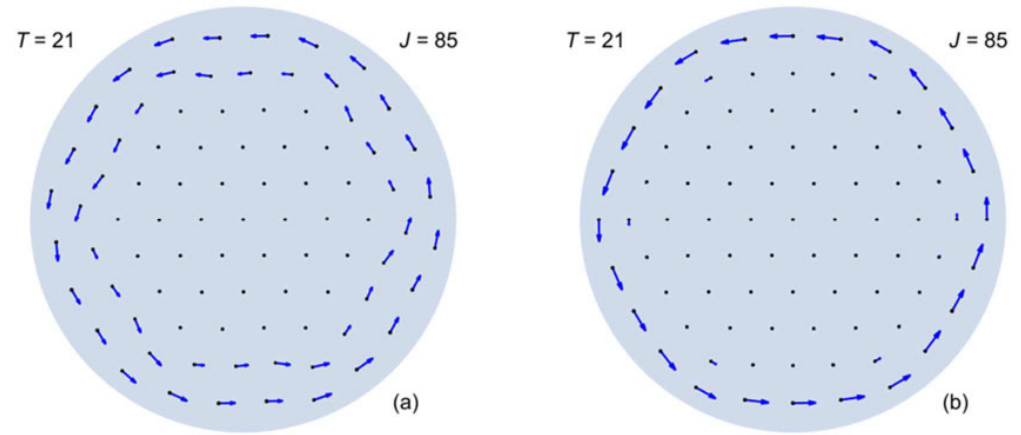

Figure 6. Differential displacements in the warped domain for generating the one-parameter families of solutions of which the configurations in Figure 4 and Figure 5 are specific members shown here in (a) and (b), respectively. A global sign change is possible on these coordinated displacements and reoptimization followed by updating the differential displacements is performed after any finite shift. Note that it is predominantly only the outermost ring that moves in (b).

The numerical values for the coordinates and weights of the sample points in the segment highlighted in Figure 4 are included as online supplement to this paper, following the format of Table 1. For the reflection-symmetric solution depicted in Figure 5, only those points in the lower right quadrant are included.

3.1.3 T=77 solution

The moderate-degree solutions presented above served to inspire the investigation of higher-degree schemes. The highest-degree cubature scheme reported in this paper is of degree 77 and is represented graphically in Figure 7 below. Like the other solutions in this section, the solution has six-fold rotational symmetry, in which case there are 507 Zernike polynomials that contribute to the residual. This solution integrates the $\binom{77+2}{2} = 3081$ monomials with just $J = 1021$ points, thereby beating our EC by six, where $\chi(77) = 1027$ and $\beta = \frac{6}{1027} = 0.6\%$. To achieve this, the scheme has one sample at the origin and 170 off-center samples per segment, leading to 510 optimization variables after the irrelevant global rotation is removed. In this case, it turns out that $\delta = 3$ and the sets of differential displacements for locally generating the family are shown in Figure 8.

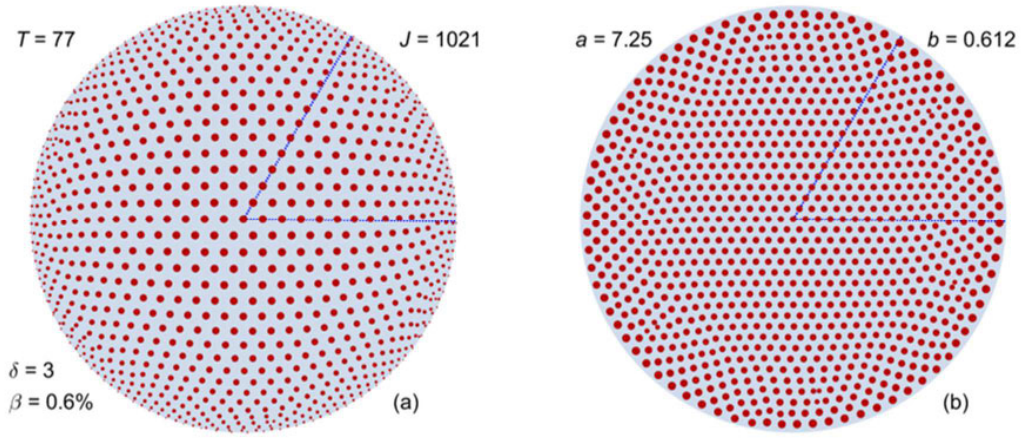

Figure 7. A cubature scheme for degree 77 using 1021 sample points with $\delta = 3$ and $\beta = 0.6\%$ is shown in (a), and the normalized depiction is in (b) with $a = 7.25$ and $b = 0.612$.

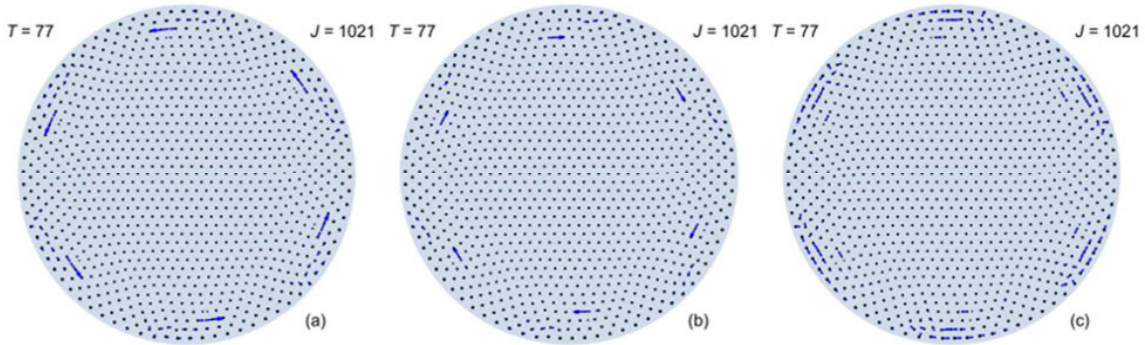

Figure 8. The differential displacements in the warped domain that locally characterize a basis for generating the three-parameter family of solutions of which the configuration in Figure 7 is a member. Notice that the displacements are primarily in the region of the points of anomalously small weights in Figure 7(b), and the motions are chiefly in the second, third, and fourth ring in from the perimeter.

Further spiraled solutions of degrees 37, 41, 53, and 65 are included in Appendix A.

3.2 Fully symmetric solutions

3.2.1 T=21 solution revisited

In some applications, it is known beforehand that the functions to be integrated possess a plane of symmetry. In such cases, plane-symmetric cubature schemes enable the estimation of these integrals by sampling over a semi-circular subset of the cubature points. It is further noted that plane-symmetric cubature schemes with k-fold rotational segmentation are automatically reflection symmetric with respect to both the x and y axes if k is even [32]. Because rotational segmentation reduces the number of points and polynomials that need to be evaluated (see Section 2.2.2), the solutions in this section also possess 2-fold rotational segmentation and are thus reflection symmetric in both x and y.

The solutions presented below were inspired by the observation that circle-packing schemes (i.e., non-overlapping arrangements of equally-sized circles within the unit disk for which increasing the radius of any single circle would cause overlap (see, e.g., [33, 34])) sometimes adopt a hexagonal pattern of isometric triangles near the center while becoming closer to a ring distribution near the edge. When the number of circles is close to (or slightly greater than) the upper bound set by our EC for a given T, circle packing schemes with these distributions can be used as initializations. For example, Figure 9 graphically represents an initial configuration for $T = 21$ whose cubature points in warped space (ω_j, θ_j) are located based on the centers of the circles in the packing scheme for $J = 85$ [35] and whose weights are calculated via Eq. (6). As can be seen in Figure 9(b), the points are approximately uniformly distributed and sized when viewed in the normalized representation discussed in Section 2.2.2.

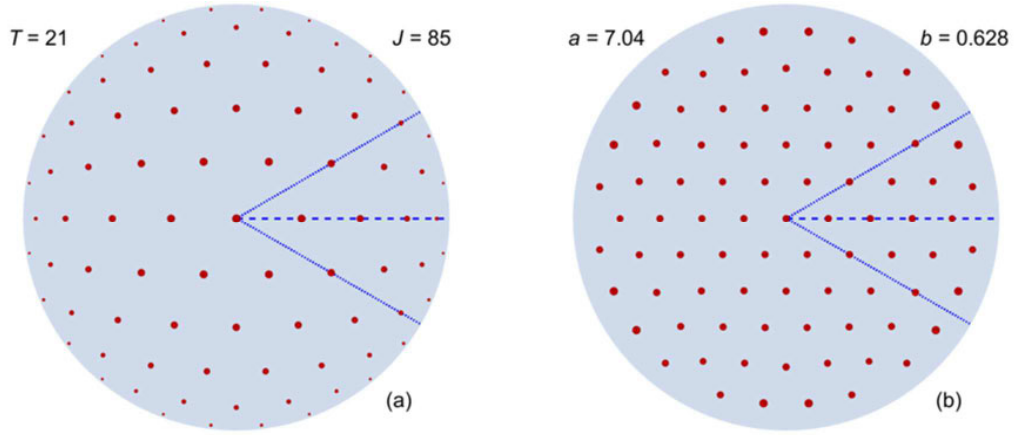

Figure 9. An initial configuration of degree 21 based on the circle-packing solution for J=85 circles is shown in (a), where the area of each point is proportional to its associated weight. The warped radial coordinate is used in (b), where the weights are normalized with $a = 7.04$ and $b = 0.628$. Because this is not an exact solution, calculations of β and δ do not apply.

The $J = 85$ packing solution had 6-fold rotational segmentation but does not quite have a plane of reflection symmetry. To create the initialization shown above, we took one half of a rotational segment, shifted the six points nearly on lines of symmetry onto those lines, and generated the full configuration via rotation and reflection. It was found that this starting point can be optimized to become a cubature solution that corresponds precisely to the plane-symmetric solution with $T = 21$ shown in Figure 5 of Section 3.1.2.

3.2.2 T=39 solution

A second, moderately high degree solution offers further guidance on the construction of the initial configuration. For $T = 39$, we require $J \leq \chi(39) = 274$. While fully symmetric solutions with 6-fold rotational segmentation do exist for moderate degrees, it was found that imposing reflection symmetry on the high-degree spiraled solutions of the previous section tended to increase the number of cubature points required to achieve exact integration beyond the upper bound set by our EC. Consequently, to facilitate the added requirement of reflection symmetry, the fully

symmetric cubature schemes presented in this paper have just two rotational segments. For degree $T = 39$, the representation in terms of Zernike polynomials yields 210 conditions that must be met.

Unlike the case for $T = 21$, no circle-packing scheme with J at or near 274 is fully symmetric. However, the $J = 284$ circle-packing solution has one axis of reflection symmetry and adopts an approximate pattern of isometric triangles near the center [36]. An initialization was generated using the north-east quadrant of this circle-packing solution.

After optimization, including many iterations of removing or consolidating cubature points, we achieved a one-parameter family of solutions with 273 cubature points in the disk, or one fewer than the upper bound set by our EC and two fewer than the solution reported in [18] (which actually fails to meet our EC). This family has 1 sample at the center, 12 samples free to vary radially along the lines of symmetry, and 62 samples within the half-segment, giving 211 optimization variables. Figure 10 depicts the solution graphically, with Figure 10(b) using the normalized representation. Figure 11 shows the differential displacements that can be used to generate the family. For all fully symmetric solutions, numerical values for the coordinates and weights of the sample points in the lower half of the segment are included as an online supplement to this paper.

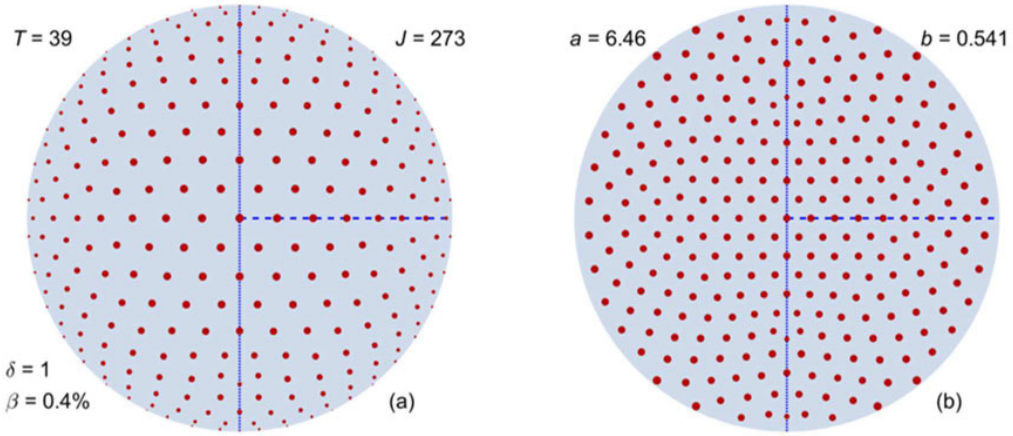

Figure 10. A symmetric cubature scheme for degree 39 using 273 sample points with $\delta = 1$ and $\beta = 0.4\%$ is shown in (a), and the normalized depiction is in (b) with $a = 6.46$ and $b = 0.541$. The dotted lines mark out one segment of the two-fold rotational symmetry, while the dashed line is the segment bisector about which the solution is reflection symmetric.

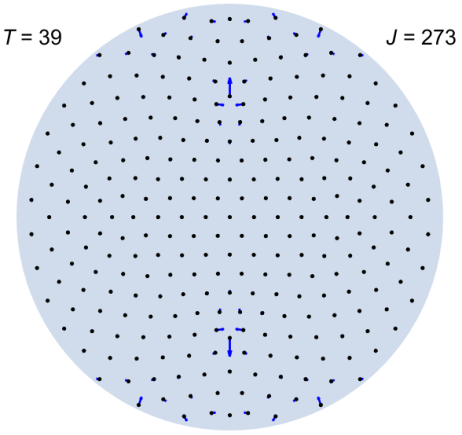

Figure 11. Differential displacements in warped coordinates for the solution in Figure 10.

3.2.3 T=53 solution

Inspired by these moderate-degree solutions, efficient cubature schemes with degrees ranging from $T = 25$ to $T = 53$ were investigated using initializations generated from circle-packing schemes. The highest-degree fully symmetric

solution is of degree 53 and is discussed here, while the remaining are in Appendix B. For $T = 53$, we seek a cubature scheme with $J \leq \chi(53) = 495$. After examining circle packing schemes for nearby values of J, the packing scheme with $J = 499$ was used to generate an initialization. With two-fold rotational segmentation and a plane of reflection symmetry, there are 378 conditions to be met.

After optimization, we achieved a two-parameter family of solutions with 495 cubature points in the disk, which is exactly $\chi(53)$. This family has one sample at the center, 17 samples free to vary radially along the lines of symmetry, and 115 samples within the half-segment, giving 380 optimization variables. Figure 12 depicts the solution graphically, with Figure 12(b) using the normalized representation. Figure 13 shows the differential displacements that can be used to generate the two-dimensional family (i.e., $\delta = 2$).

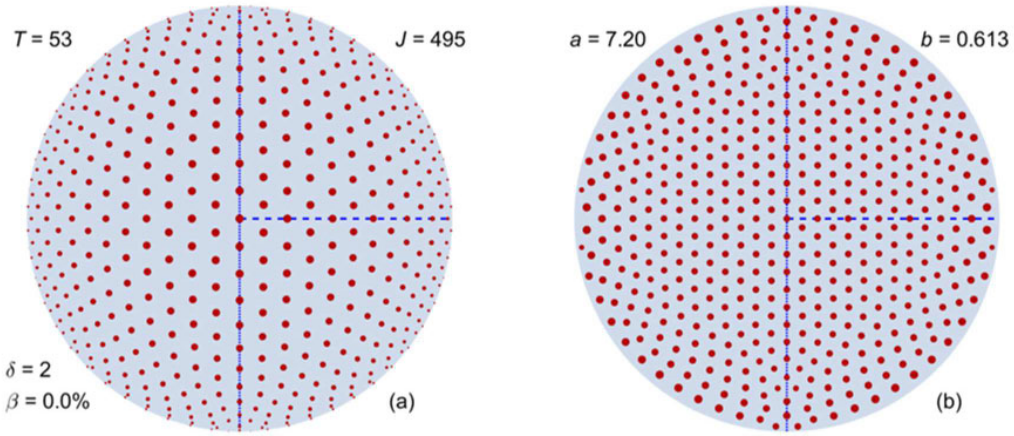

Figure 12. A cubature scheme for degree 53 using 495 sample points with $\delta = 2$ and $\beta = 0\%$ is shown in (a), and the normalized depiction is in (b) with $a = 7.20$ and $b = 0.613$.

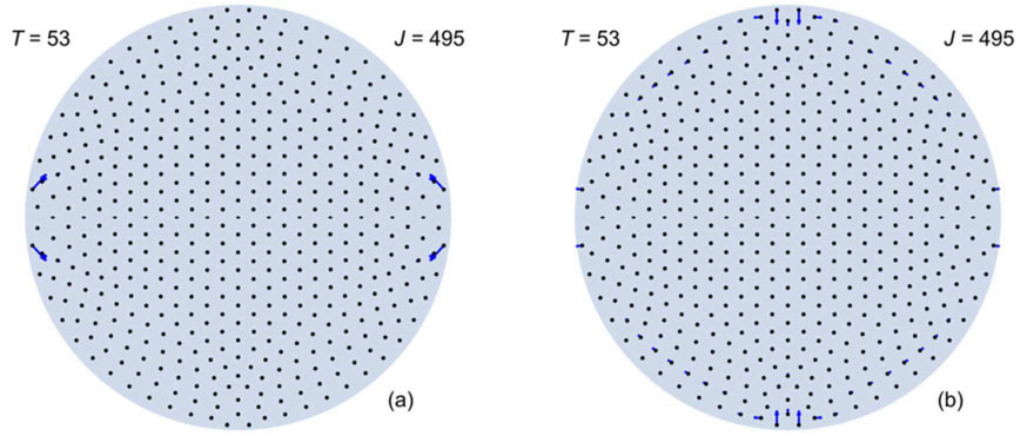

Figure 13. Differential displacements in warped coordinates for the solution in Figure 12.

4 Discussion

In this paper, moderate-to-high degree cubature schemes were reported that either meet or outperform a simple efficiency criterion on the number of cubature points. These cubature schemes, whose coordinates and weights are provided explicitly to facilitate numerical integration in an online supplement to this publication, range from a degree-17 scheme using only 55 cubature points to the degree-77 scheme with over one thousand points.

Heuristics for selecting initializations and guiding the optimization process were also discussed, such as the visualization of cubature schemes in warped coordinates with each point's area proportional to its normalized weight. By following these heuristics, cubature schemes were found that tended to adopt a hexagonal pattern of isometric triangles near the center and an approximately circular pattern of rings near the edge. In interpreting this observation, it is noted that the hexagonal pattern is suggestive of the hexagonal lattices that optimally pack equal-area circles in the unit plane (see, e.g., [33]). Similarly, the approximately circular pattern of rings near the edge corresponds to an approximately uniform sampling of the circular boundary. This connection to circle packing schemes inspired their use to generate initializations in Section 3.2, which were effective at creating the solutions in Appendix B.

Although these optimization heuristics successfully facilitated the discovery of the schemes reported in this paper, it is important to note that they were developed concurrently with those results: the heuristics enabled the results, which, in turn, refined the heuristics. However, the results in this paper should not be interpreted as ruling out other distributions. While a full exploration of alternative optimization heuristics and cubature point distributions is beyond the scope of this paper, we include one anomalous distribution, of degree 37, that was constructed by using an initial configuration inspired by Chebyshev lattices for cubature on the unit square [37, 38]. Like the degree-37 cubature scheme in Figure 24 of Appendix B, this solution uses 245 cubature points to integrate 741 monomials, meaning that it beats our EC of $J \leq \chi(37) = 247$ by two. This cubature scheme is represented graphically in Figure 14, in which it can be seen to have an approximately square lattice distribution near the center (oriented at 45 degrees) and a roughly circular pattern of rings near the edge. Examining alternative heuristics such as this, including whether they can be leveraged to yield cubature schemes with even fewer cubature points, is an enticing topic for future research.

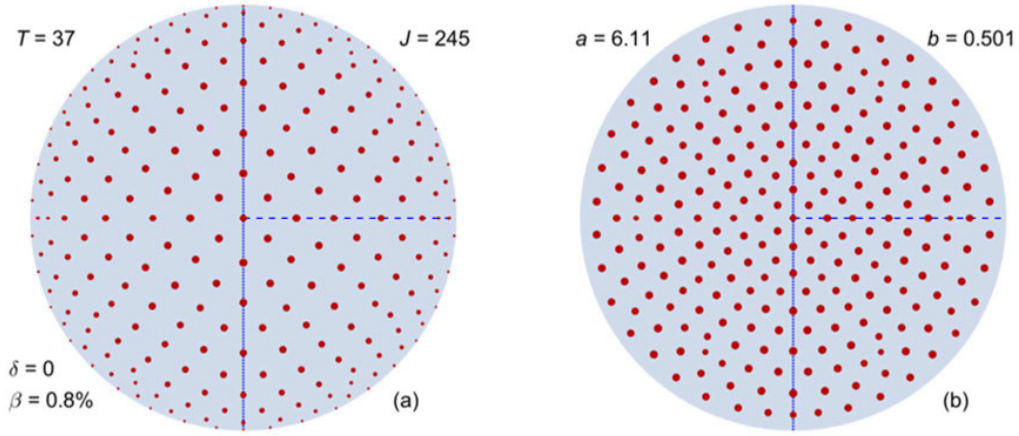

Figure 14. In the representation used in Section 3, a cubature scheme for degree 37 using 245 cubature points with $\delta = 0$ and $\beta = 0.8\%$ is shown in (a) and the normalized depiction is in (b) with $a = 6.11$ and $b = 0.501$.

As another tool to give an easier appreciation of and insights into the configurations that emerge in the cubature schemes of this paper, we have found it rewarding to examine the Voronoi tessellations of the unit disk in warped space, in which each cell is colored according to a measure of the number of edges on the cell. Because a simplistic edge count is sensitive to vanishingly small edges, we have found it more helpful and robust to use the square of the cell's perimeter divided by the sum of the squares of the edge lengths. This measure is exactly equal to the number of edges when all edges have equal length and continuously accounts for shrinking or growing edges to give a more effective nominal edge count. Some examples are presented in Figure 15. Given that decorations of the circle are ubiquitous in nature, art, craft, and culture, these striking patterns bring to mind many topics such as compound insect eyes, floral seed structures, doilies, mandalas, cathedral windows, and mosque ceilings.

In these color-coded Voronoi tessellations, the patterns in many cases, such as the hexagonal pattern of isometric triangles adopted near the center, are visually apparent as areas of uniformly colored cells. Likewise, transitions between such configurations, such as the transition from the hexagonal pattern near the center to the circular pattern around the edge, are represented via intermediately colored cells. Sample points that are inconsistent with their neighbors' configuration appear as blemishes in this representation and may suggest areas of improvement. For

example, the blemishes in the degree-77 scheme in Figure 15(e) call out for a continued search to find a solution with $J = 1015$ that is a worthy partner to the elegant, isolated degree-17 solution in Figure 15(d). That is, if the three redundant parameters discussed in Section 3.1.3 could lead to the removal of one point from each of the six rotational segments, then the three-dimensional family with $J = 1021$ would become an isolated solution with $J = 1015$, $\delta = 0$ and $\beta = 1.2\%$.

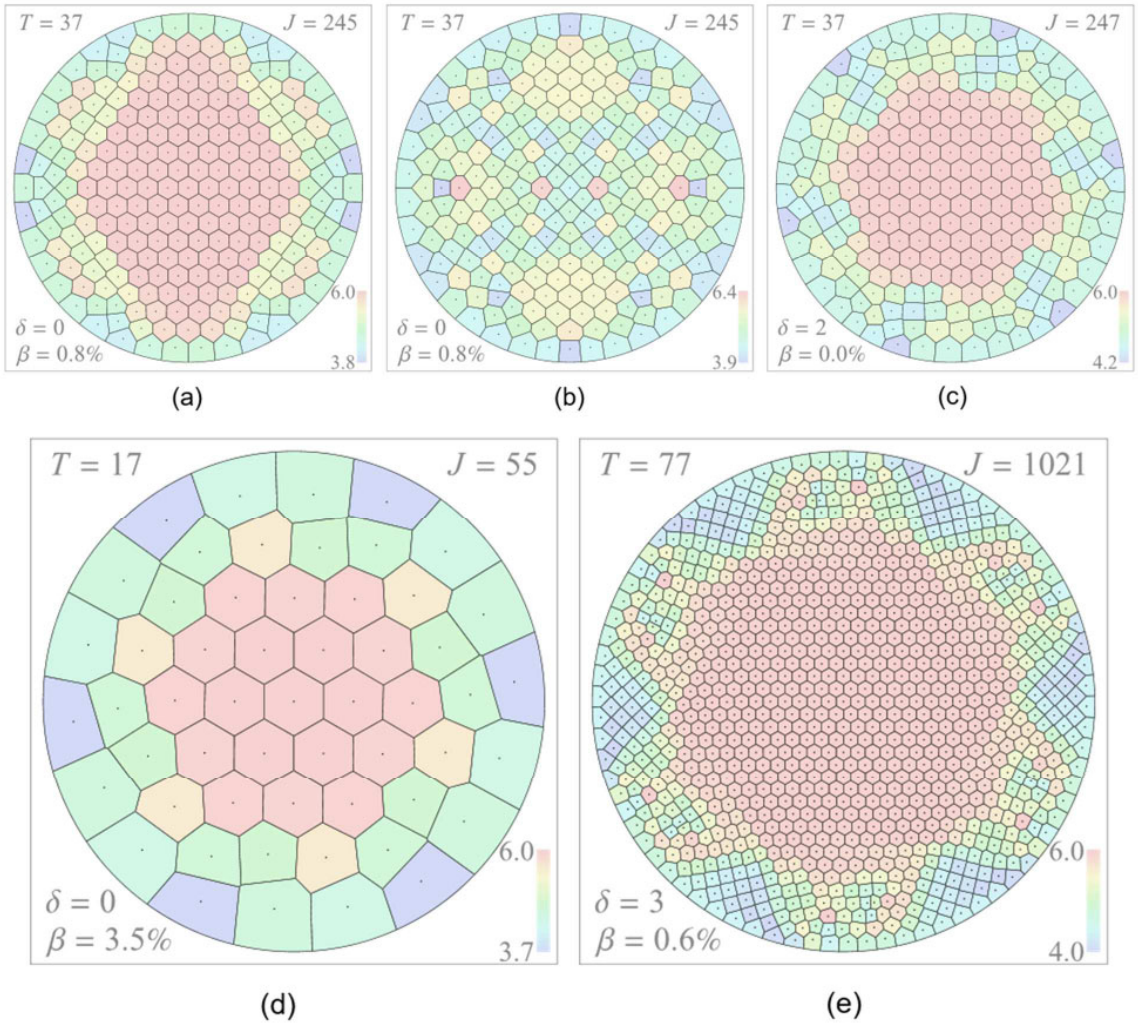

Figure 15. Color-coded Voronoi tessellations for a selection of the cubature schemes reported here. In (a), (b), and (c), the tessellations are for degree-37 solutions with hexagonal, Chebyshev, and spiraled patterns, respectively. In (d) and (e), tessellations for spiraled solutions for degrees 17 and 77, respectively. The hue varies from red to blue as the measure of edge count falls from maximum to minimum. The color transition in the legend represents a linear scale between the displayed extreme values. Notice that the scheme in (b) is the outlier discussed in Figure 14 that has a more rectangular arrangement (aligned at 45 degrees) near its center and has four cells with notably high effective edge count.

Although the results presented in this paper have focused on cubature of the unit disk, it is interesting to consider how similar techniques will fare at generating cubature schemes for other domains of integration. It is intriguing to see if optimization heuristics will differ for domains of integration with high aspect ratios. For example, it may be possible to construct initial configurations for cubature of the rectangle by viewing 1D quadrature solutions as cubature schemes over a rectangle of sufficiently high aspect ratio and then progressively reducing that ratio. Having done so, a similar construction may be possible for ellipsoidal domains, which may give insights if contrasted with distributions

for cubature over the unit disk. These particular shapes are by no means exhaustive: other domains of integration are of interest in various disciplines, and it would be fascinating to compare trends in solutions across different domains.

While the results presented in this paper represent the best efforts of the authors to achieve cubature schemes with fewest sample points for given degrees, the search for further improvements is bound to be rewarding. It is almost certain that tailored optimization approaches and/or greater computational resources can be leveraged to discover schemes of even higher degree or with fewer sample points. We envision that other researchers who are algorithm specialists may be intrigued by the results that we report and be attracted to find better ways to derive these and related solutions.

5 Appendix A: Gallery of spiraled schemes

The spiraled solutions discussed in Section 3.1 are further supplemented by spiraled solutions of degrees 37, 41, 53, and 65. Like the solutions in Section 3.1, all solutions adopt six-fold rotational segmentation, meet or exceed our EC (as reported by β), and are shown visually, including a normalized depiction. Numerical values for the coordinates and weights of the points in the marked segment for each of these solutions are provided in an online supplement to this paper. Differential displacements for locally generating families of solutions are not provided due to length considerations, but the dimensions of those families are reported by δ.

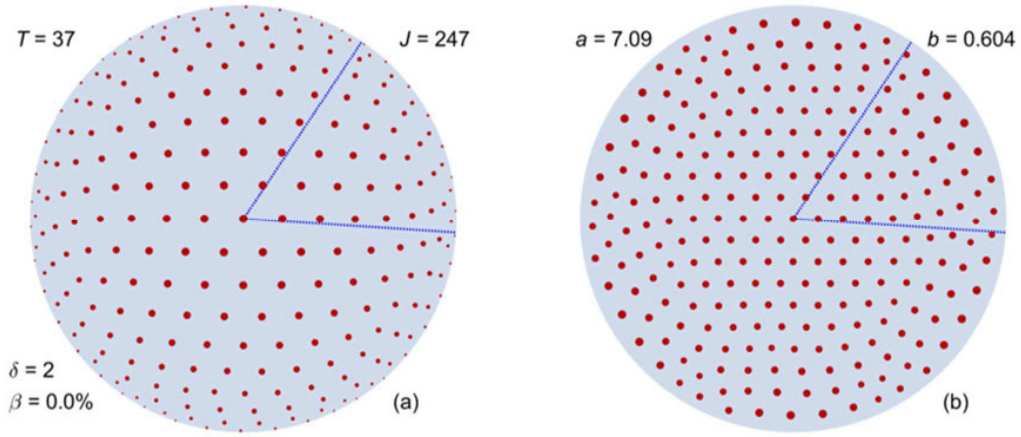

Figure 16. A cubature scheme for degree 37 using 247 sample points with $\delta = 2$ and $\beta = 0\%$ is shown in (a), and the normalized depiction is in (b) with $a = 7.09$ and $b = 0.604$. This solution exactly meets the target set by $\chi(T) = 247$.

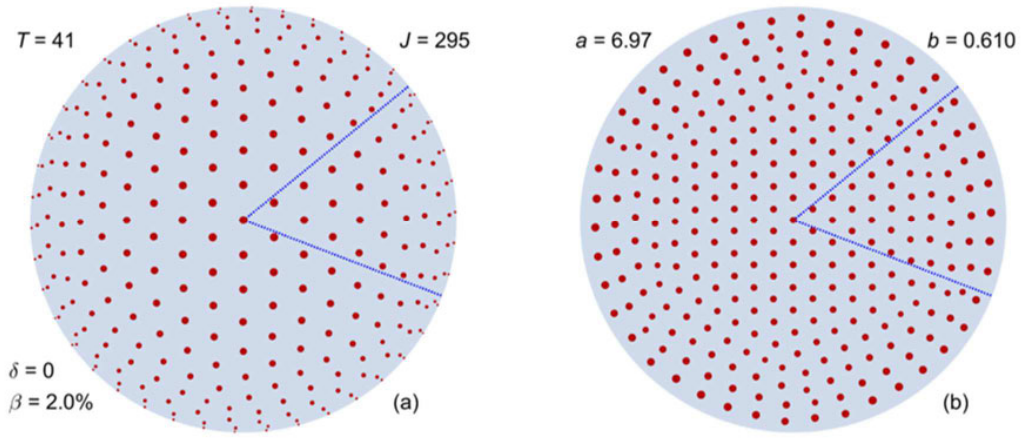

Figure 17. A cubature scheme for degree 41 using 295 sample points with $\delta = 0$ and $\beta = 2.0\%$ is shown in (a), and the normalized depiction is in (b) with $a = 6.97$ and $b = 0.610$. This solution beats the target set by $\chi(T) = 301$ by six.

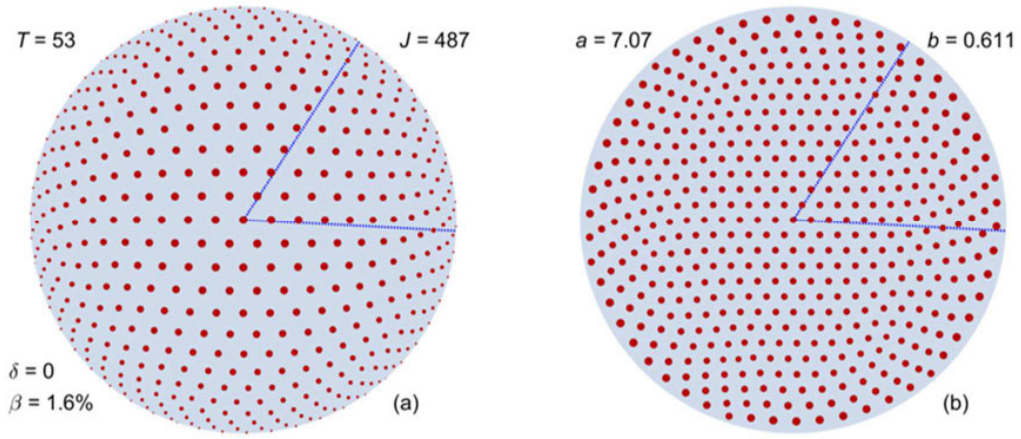

Figure 18. A cubature scheme for degree 53 using 487 sample points with $\delta = 0$ and $\beta = 1.6\%$ is shown in (a), and the normalized depiction is in (b) with $a = 7.07$ and $b = 0.611$. This solution beats the target set by $\chi(T) = 495$ by eight.

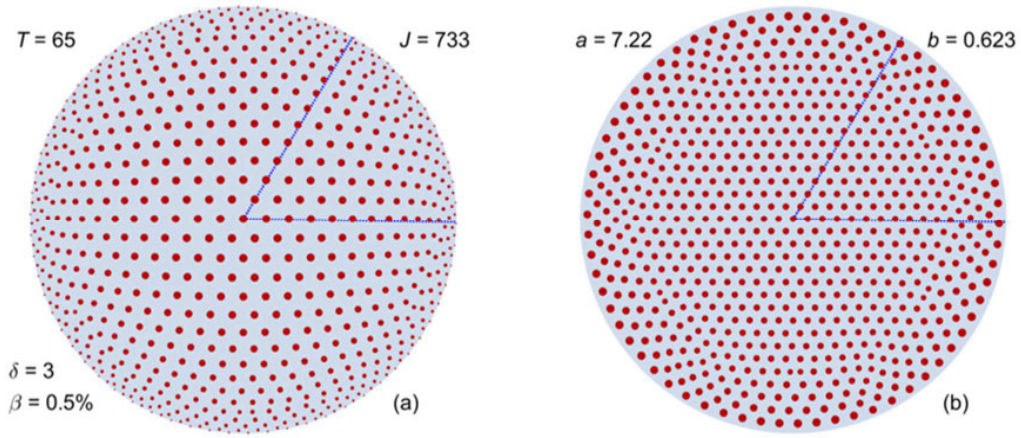

Figure 19. A cubature scheme for degree 65 using 733 sample points with $\delta = 3$ and $\beta = 0.5\%$ is shown in (a), and the normalized depiction is in (b) with $a = 7.22$ and $b = 0.623$. This solution beats the target set by $\chi(T) = 737$ by four.

6 Appendix B: Gallery of fully symmetric schemes

Fully symmetric schemes of degree 39 and 53 were discussed in Section 3.2. Additional schemes are graphically represented in this section. While these solutions are not given individual discussion, it is noted that they all meet or beat our EC (as reported by β). In addition to those presented in this section, cubature schemes adopting similar patterns to those below were found for each odd degree ranging from 23 to 55 that does not have an associated cubature scheme below, but these solutions exceed $\chi(T)$ by one or two sample points and consequently are not included. Numerical values for the coordinates and weights of the points in the lower-right quadrant for each of these solutions are provided as an online supplement to this paper. As with the spiraled solutions in Appendix A, differential displacements for locally generating families of solutions are not provided due to length considerations, but the dimensions of those families are reported by δ.

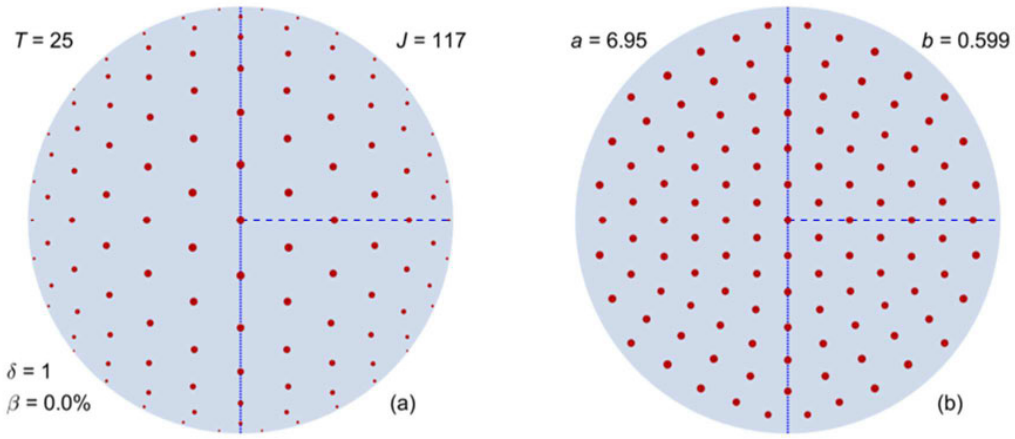

Figure 20. A fully symmetric cubature scheme of degree 25 using 117 sample points with $\delta = 1$ and $\beta = 0.0\%$ is shown in (a), and the normalized depiction with $a = 6.95$ and $b = 0.599$. This solution exactly meets the target set by $\chi(T) = 117$.

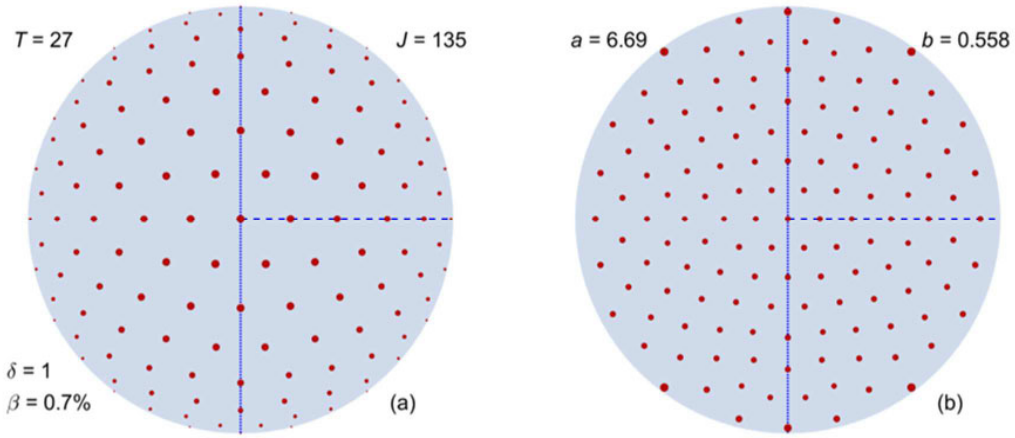

Figure 21. A fully symmetric cubature scheme of degree 27 using 135 sample points with $\delta = 1$ and $\beta = 0.7\%$ is shown in (a), and the normalized depiction with $a = 6.69$ and $b = 0.558$. This solution beats the target set by $\chi(T) = 136$ by one.

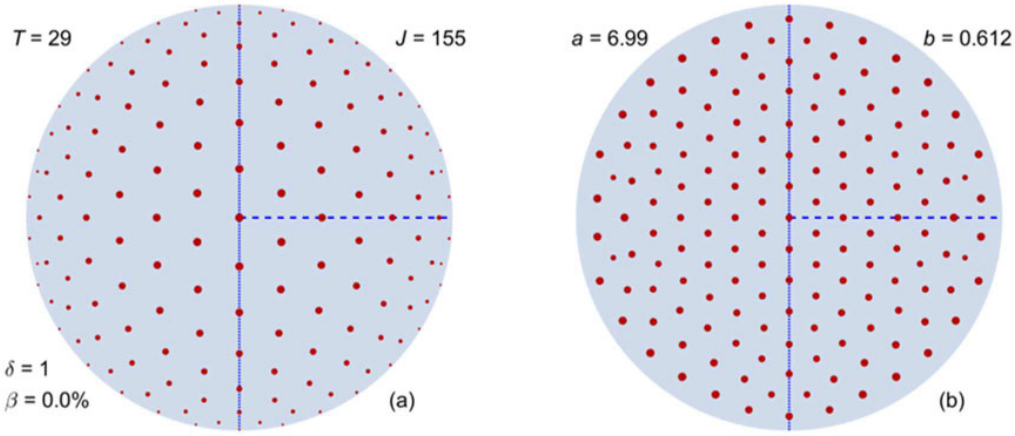

Figure 22. A fully symmetric cubature scheme of degree 29 using 155 sample points with $\delta = 1$ and $\beta = 0\%$ is shown in (a), and the normalized depiction with $a = 6.99$ and $b = 0.612$. This solution exactly meets the target set by $\chi(T) = 155$.

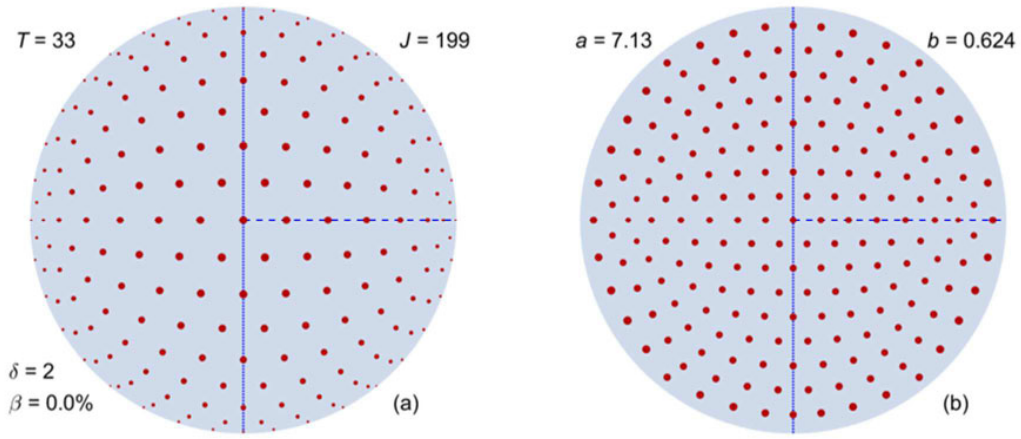

Figure 23. A fully symmetric cubature scheme of degree 33 using 199 sample points with $\delta = 2$ and $\beta = 0\%$ is shown in (a), and the normalized depiction with $a = 7.13$ and $b = 0.624$. This solution exactly meets the target set by $\chi(T) = 199$.

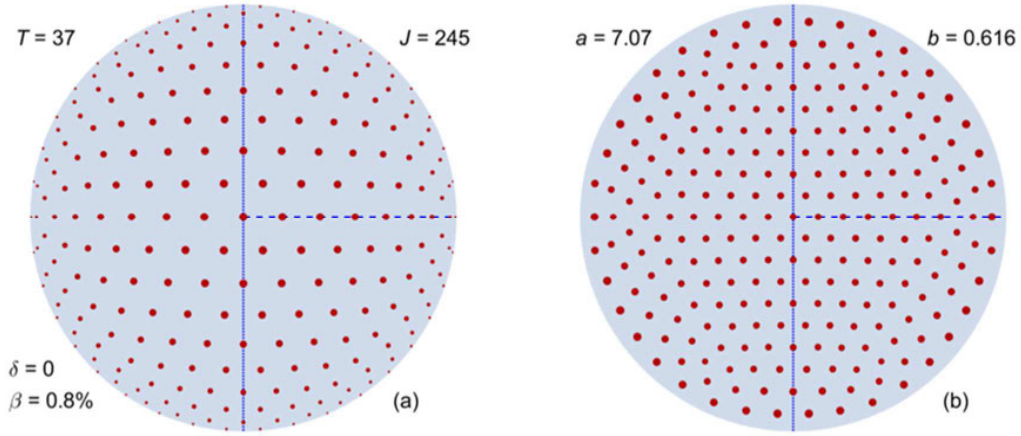

Figure 24. A fully symmetric cubature scheme of degree 37 using 245 sample points with $\delta = 0$ and $\beta = 0.8\%$ is shown in (a), and the normalized depiction with $a = 7.07$ and $b = 0.616$. This solution beats the target set by $\chi(T) = 247$ by two.

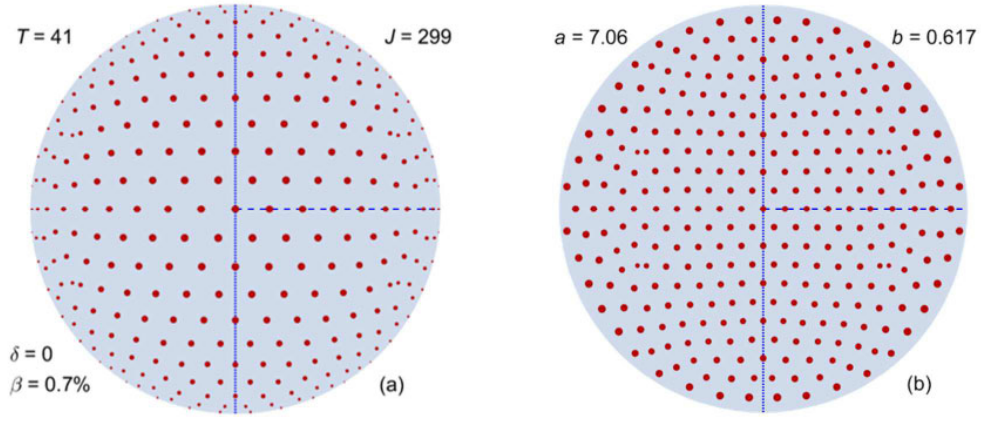

Figure 25. A fully symmetric cubature scheme of degree 41 using 299 sample points with $\delta = 0$ and $\beta = 0.7\%$ is shown in (a), and the normalized depiction with $a = 7.06$ and $b = 0.617$. This solution beats the target set by $\chi(T) = 301$ by two.

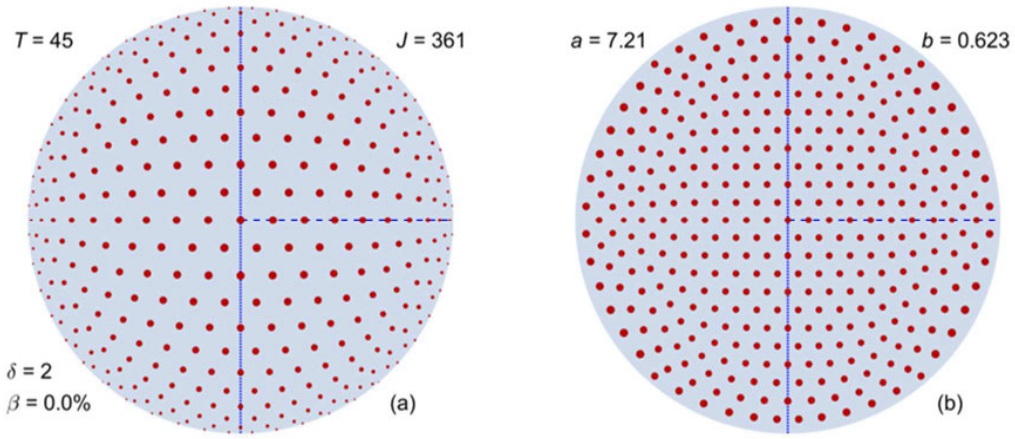

Figure 26. A fully symmetric cubature scheme of degree 45 using 361 sample points with $\delta = 2$ and $\beta = 0\%$ is shown in (a), and the normalized depiction with $a = 7.21$ and $b = 0.623$. This solution exactly meets the target set by $\chi(T) = 361$.

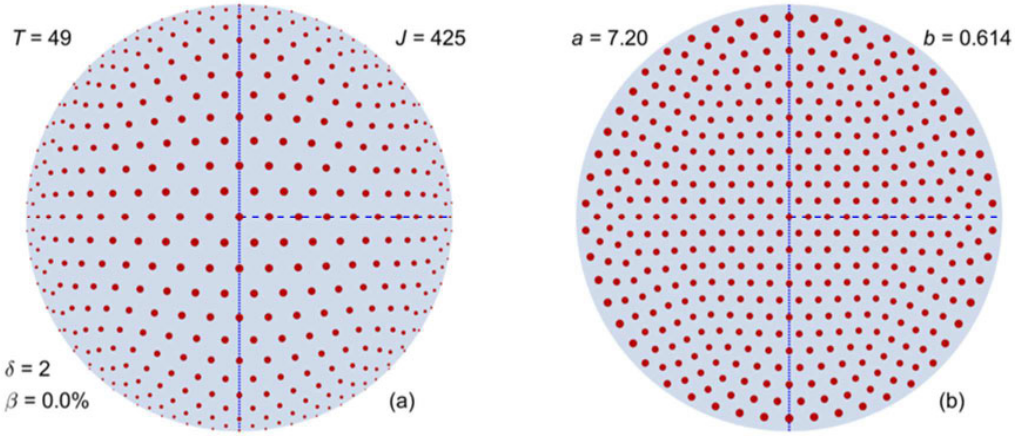

Figure 27. A fully symmetric cubature scheme of degree 49 using 425 sample points with $\delta = 2$ and $\beta = 0\%$ is shown in (a), and the normalized depiction with $a = 7.20$ and $b = 0.614$. This solution exactly meets the target set by $\chi(T) = 425$.

7 Appendix C: Calculating Differential Displacements

In Section 2.2.3, it was remarked that differential displacements that preserve the error value of zero to second order were often found for a zero-error solution if the number of optimization variables exceeds the number of polynomials contributing to the residual. These differential displacements are exactly the null eigenvectors of the approximate Hessian $\boldsymbol{J}(\boldsymbol{u})^T\boldsymbol{J}(\boldsymbol{u})$ associated with the square error function $E^2(\boldsymbol{u}) = \boldsymbol{R}(\boldsymbol{u})^T\boldsymbol{R}(\boldsymbol{u})$ defined in Eq. (4), where, for ease of notation, $\boldsymbol{u}$ is used as the current set of points and weights and $\boldsymbol{J}$ represents the Jacobian of the residuals.

To see that these null eigenvectors do indeed preserve the zero-error solution to second order, we note that the Taylor expansion of E^2 at a zero-error solution $\boldsymbol{u_0}$ with a displacement $\boldsymbol{h}$ is

$$E^2(\boldsymbol{u_0} + \boldsymbol{h}) = E^2(\boldsymbol{u_0}) + \boldsymbol{h} \cdot \nabla E^2(\boldsymbol{u_0}) + \tfrac{1}{2}\boldsymbol{h}^T\boldsymbol{H}(\boldsymbol{u_0})\boldsymbol{h} + O(|\boldsymbol{h}|^3), \tag{12}$$

which, because $E^2(\boldsymbol{u_0}) = 0$ and $\nabla E^2(\boldsymbol{u_0}) = 2\nabla(\boldsymbol{R}^T\boldsymbol{R})(\boldsymbol{u_0}) = 2\boldsymbol{J}(\boldsymbol{u_0})^T\boldsymbol{R}(\boldsymbol{u_0}) = 0$, is simply $\frac{1}{2}\boldsymbol{h}^T\boldsymbol{H}(\boldsymbol{u_0})\boldsymbol{h} + \boldsymbol{O}(|\boldsymbol{h}|^3)$. Note that $\boldsymbol{H}$ is used as the exact Hessian for E^2.

It follows that, if $\boldsymbol{h}$ is a zero-value eigenvector of $\boldsymbol{H}(\boldsymbol{u_0})$, then $E^2(\boldsymbol{u_0}+\boldsymbol{h})$ is zero to second order. Because $\boldsymbol{H}(\boldsymbol{u_0})$ is the Hessian of a square error function evaluated at a zero-error solution, $\boldsymbol{H}(\boldsymbol{u_0}) = 2\,\boldsymbol{J}(\boldsymbol{u_0})^T\boldsymbol{J}(\boldsymbol{u_0})$ (this fact is well-known for least-squares problems; see, for example, [39]).

Consequently, the null eigenvectors of $\boldsymbol{J}(\boldsymbol{u_0})^T\boldsymbol{J}(\boldsymbol{u_0})$ can be used as differential displacements. By displacing a zero-error solution by a small amount along these differential displacements and reoptimizing, we found that similar solutions could be achieved that differed from the original solution by approximately the differential displacement.

When seeking the solutions reported in this paper, routines such as the EIG routine in MATLAB were used to calculate these differential displacements [40].

8 Appendix D: Numerical test of exactness for the T=17 solution

As a test of exactness, the full cubature scheme of degree 17 presented in Table 1 was used to estimate the integral of the polynomial $C_1P_3^{(0,4)}(2u^2-1)u^4\sin(4\theta)+C_2P_8^{(0,0)}(2u^2-1)+C_3P_2^{(0,5)}(2u^2-1)u^5\cos(5\theta)$. The coefficients $C_1 = 0.792207329559754$, $C_2 = 0.035711678574569$ and $C_3 = 0.678735154857380$ were chosen uniformly at random from within [0,1] by the RAND function in MATLAB [41]. The Zernike polynomials were also chosen at random, with the requirement that one term must have sinusoidal azimuthal dependence, one term must have cosinusoidal azimuthal dependence, and one term is rotationally invariant.

The square error of estimating the value of this integral is approximately 2.7×10^{-32}, which is representative of the performance of the other cubature schemes presented in this paper. MATLAB code for reading cubature schemes and examining their performance for single Zernike polynomial is provided as a supplement to this paper.

References

[1] A.H. Stroud, Approximate Calculation of Multiple Integrals, Prentice-Hall, 1971.
[2] H.M. Möller, Kubaturformeln mit minimaler Knotenzahl, Numerische Mathematik, 25 (1976) 185-200.
[3] B. Benouahmane, A. Cuyt, Multivariate orthogonal polynomials, homogeneous Pade approximants and Gaussian cubature, Numerical Algorithms, 24 (2000) 1-15.
[4] Y. Xu, Minimal cubature rules and polynomial interpolation in two variables, Journal of Approximation Theory, 164 (2011) 6-30.
[5] B. Benouahmane, A. Cuyt, I. Yaman, Near-minimal cubature formulae on the disk, IMA Journal of Numerical Analysis, 39 (2017) 297-314.
[6] H.J. Schmid, Y. Xu, On bivariate Gaussian cubature formulae, Proceedings of the American Mathematical Society, 122 (1994) 833-841.
[7] S. Heo, Y. Xu, Constructing cubature formulae for spheres and balls, Journal of Computational and Applied Mathematics, 112 (1999) 95-119.
[8] G. Petrova, Cubature formulae for spheres, simplices and balls, Journal of Computational and Applied Mathematics, 162 (2004) 483-496.
[9] H. Li, J. Sun, Y. Xu, Discrete Fourier Analysis, Cubature, and Interpolation on a Hexagon and a Triangle, SIAM Journal on Numerical Analysis, 46 (2008).
[10] H. Nguyen, G. Petrova, Extended Gaussian type cubatures for the ball, Journal of Computational and Applied Mathematics, 290 (2015) 209-223.
[11] S.-A. Papanicolopulos, New fully symmetric and rotationally symmetric cubature rules on the triangle using minimal orthonormal bases, Journal of Computational and Applied Mathematics, 294 (2016) 39-48.
[12] B. Bauman, A. Sommariva, M. Vianello, Compressed algebraic cubature over polygons with applications to optical design, Journal of Computational and Applied Mathematics, 370 (2020) 112658.
[13] Y. Xu, Orthogonal polynomials and cubature formulae on balls, simplices, and spheres, Journal of Computational and Applied Mathematics, 127 (2001) 349-368.

[14] R. Cools, K.-J. Kim, A survey of known and new cubature formulas for the unit disk, Korean Journal of Applied Mathematics and Computing, 7 (2000) 477-485.
[15] K.-J. Kim, M.-S. Song, Symmetric quadrature formulas over a unit disk, Korean Journal of Applied Mathematics and Computing, 4 (1997) 172-192.
[16] R. Cools, An encyclopaedia of cubature formulas, Journal of Complexity, 19 (2003) 445-453.
[17] G. Forbes, J. Ruoff, A. Flesch, N. Kerwien, Ray selection for optimization of rotationally symmetric systems, Advanced Optical Technologies, 5 (2016) 237-247.
[18] G. Forbes, J. Ruoff, Rapid evaluation of vignetting-free high-performance systems, Optical Engineering, 57 (2018) 101709.
[19] M. Taylor, B. Wingate, L. Bos, A Cardinal Function Algorithm for Computing Multivariate Quadrature Points, SIAM J. Numerical Analysis, 45 (2007) 193-205.
[20] S.-A. Papanicolopulos, Efficient computation of cubature rules with application to new asymmetric rules on the triangle, Journal of Computational and Applied Mathematics, 304 (2016) 73-83.
[21] L. Zhang, T. Cui, H. Liu, A set of symmetric quadrature rules on triangles and tetrahedra, Journal of Computational Mathematics, 27 (2009) 89-96.
[22] F.D. Witherden, P.E. Vincent, On the identification of symmetric quadrature rules for finite element methods, Computers & Mathematics with Applications, 69 (2015) 1232-1241.
[23] E.W. Weisstein, "Moore-Penrose Matrix Inverse" (from Mathworld - A Wolfram Web Resource), retrieved November 29, 2021, https://mathworld.wolfram.com/Moore-PenroseMatrixInverse.html.
[24] Wolfram Research, "LinearSolve" (1988), retrieved November 29, 2021, https://reference.wolfram.com/language/ref/LinearSolve.html (updated 2014).
[25] The MathWorks Inc., "pinv - Moore-Penrose pseudoinverse" (2021), retrieved November 29, 2021, https://www.mathworks.com/help/matlab/ref/pinv.html.
[26] The MathWorks Inc., "lsqnonlin - Solve nonlinear least-squares (nonlinear data-fitting) problems" (2021), retrieved November 29, 2021, https://www.mathworks.com/help/optim/ug/lsqnonlin.html.
[27] F. Zernike, Beugungstheorie des schneidenver-fahrens und seiner verbesserten form, der phasenkontrastmethode, Physica, 1 (1934) 689-704.
[28] E.W. Weisstein, "Zernike Polynomials" (from MathWorld - A Wolfram Web Resource), retrieved October 30, 2018, https://mathworld.wolfram.com/ZernikePolynomial.html.
[29] G.W. Forbes, Robust and fast computation for the polynomials of optics, Optics Express, 18 (2010) 13851-13862.
[30] E.W. Weisstein, "Jacobi Polynomials" (from MathWorld - A Wolfram Web Resource), retrieved October 30, 2018, http://mathworld.wolfram.com/JacobiPolynomial.html.
[31] P.J. David, I. Polonsky, Numerical Interpolation, Differentiation, and Integration, in: M. Abramowitz, I.A. Stegun (Eds.) Handbook of Mathematical Functions with Formulas, Graphs, and Mathematical Tables, United States Department of Commerce, National Bureau of Standards New York, 1972, pp. 889.
[32] R. Cools, Constructing cubature formulae: the science behind the art, Acta Numerica, 6 (1997) 1-54.
[33] E.W. Weisstein, "Circle Packing" (from MathWorld - A Wolfram Web Resource), retrieved October 26, 2020, https://mathworld.wolfram.com/CirclePacking.html.
[34] E. Specht, "The best known packings of equal circles in a circle" (Otto von Guericke University Magdeburg, 2018), retrieved October 26, 2020, http://hydra.nat.uni-magdeburg.de/packing/cci/cci.html#overview.
[35] J. Donovan, "N=85" (Otto von Guericke University Magdeburg, 2018), retrieved October 26, 2020, http://hydra.nat.uni-magdeburg.de/packing/cci/d8.html.
[36] D.W. Cantrell, "N=284" (Otto von Guericke University Magdeburg, 2008), retrieved October 26, 2020, http://hydra.nat.uni-magdeburg.de/packing/cci/d24.html.
[37] L. Bos, M. Caliari, S. De Marchi, M. Vianello, Y. Xu, Bivariate Lagrange interpolation at the Padua points: The generating curve approach, Journal of Approximation Theory, 143 (2006) 15-25.

[38] R. Cools, K. Poppe, Chebyshev lattices, a unifying framework for cubature with Chebyshev weight function, BIT Numerical Mathematics, 51 (2011) 275-288.
[39] R. Kress, Least Square Problems, in: Numerical Analysis, Springer-Verlag New York, Inc., New York, 1998, pp. 114-118.
[40] The MathWorks Inc., "eig - Eigenvalues and eigenvectors" (2021), retrieved November 29, 2021, https://www.mathworks.com/help/matlab/ref/eig.html.
[41] The MathWorks Inc., "rand - Uniformly distributed random numbers" (2021), retrieved November 29, 2021, https://www.mathworks.com/help/matlab/ref/rand.html.